NJC

Accepted Manuscript

This is an *Accepted Manuscript*, which has been through the Royal Society of Chemistry peer review process and has been accepted for publication.

Accepted Manuscripts are published online shortly after acceptance, before technical editing, formatting and proof reading. Using this free service, authors can make their results available to the community, in citable form, before we publish the edited article. We will replace this *Accepted Manuscript* with the edited and formatted *Advance Article* as soon as it is available.

You can find more information about *Accepted Manuscripts* in the **Information for Authors**.

ROYAL SOCIETY OF CHEMISTRY

www.rsc.org/njc

Journal Name

ARTICLE

A facile method for synthesis of Co-core Au-shell nanohybrid

Debasmita Sardar,[a,b] S. K. Neogi,[b,c] S. Bandyopadhyay,[b,c] Biswarup Satpati,[d] Ruchi Jain,[e] Chinnakonda S. Gopinath,[e] and Tanushree Bala [a,b] *

Heterostructured Co-Au core-shell nanoparticles have been synthesized by reducing $AuCl_4^-$ ion on Cobalt nanoparticles after a minor but effective modification of Cobalt surface modification by an amine. The core shell morphology is emphatically confirmed by the thorough investigation through UV-Vis spectroscopy, X-ray Photoelectron Spectroscopy (XPS), Transmission Microscopic Analysis (TEM). The chemical composition and topography are determined using STEM-HAADF analysis and EFTEM imaging. The Fourier Transform Infrared (FTIR) spectroscopy proves the surface modification of Co nanoparticle and the interactions involved between the ligands with core and shell metals at various steps of the synthetic process. Magnetic property confirms the material to be superparamagnetic in nature.

Introduction:

Current literature has been flooded with physical and chemical recipes towards the synthesis of structures like spherical nanoparticles,[1,2] nanowires,[3,4] nanorods,[5,6] nanoprisms,[5,7] nanotubes[8] etc, owing to the fundamental study of property-size based relationship along with diverse application potential. Among various groups of nanomaterials, magnetic nanostructures[9,10] over the decade have grabbed considerable amount of attention due to its potential application in optics,[9,11,12] electronics,[13] catalysis,[14] targeted drug delivery systems[15] and so on. The superparamagnetic[16] property of the magnetic nanostructures is found imperative for biomedical applications such as cell separation,[17] biosensors,[11] hyperthermia of tumours and MRI technique.[18] While synthesis has been predominant, the trickiest part is to generate non-agglomerated magnetic nanoparticles which are stable against aerial oxidation. In particular, the magnetic metallic (Co, Ni, Fe)[19] nanoparticles are extremely prone towards oxidation rendering only scarce number of literature reports for their synthesis. Enveloping the particles in a shell of noble metal has served a route to overcome the quandary and synthesizing these nanoparticles in organic medium[20] with suitable ligands is another common way-out. Though organic-medium based synthesis can avoid aerial oxidation, here the particles strive severe limitation towards their application for biological purpose.[21] This is definitely a loophole for the synthesis of magnetic nanomaterials in organic medium. Moreover the use of toxic solvents,[20,22] high temperature[23] and sophisticated experimental setup make the synthesis process further complicated. On the other hand, aqueous phase based techniques involves mainly reverse micelle based methods

where yield of the product is relatively low. Very recently Prasad and co-workers have reported a facile water based technique to generate monodispersed magnetic nanoparticles.[24] The surfactants present on the surface of these nanoparticles can stabilize the particle against immediate aerial oxidation but the formation of layers of oxide cannot be overruled completely with time.[25] The stability and biocompatibility both can be improved for these particles by creating a bio-friendly interface on magnetic nanoparticles by growing a gold shell. Gold coated magnetic particles have been reported in plenty. However use of strong reducing agents (e.g. $NaBH_4$)[26] in aqueous medium or carrying out the reaction in organic medium has their own merits and demerits. Cheon and his group have reported organic phase based Au-shell formation under reflux condition using TOP as capping agent. The use of uncommon chemical-stabilizer, inert atmosphere[27] or non-green solvents[28] still furnishes lacuna in this regard.

Thus here in this paper we report the conversion of water based cobalt nanoparticles to a stable core-shell system by creating a gold shell via an amine mediated reduction method. The pristine cobalt nanoparticles have surfactants on the surface which are replaced probably partially by an amino acid L-Tryptophan (Trp). This in turn can act as the reducing agent yielding Co-core Au-shell nanostructures. It is envisaged that core–shell structures of Co-core and Au-shell, will not only render the cobalt nanoparticles more robust chemically but also provide the manipulative ability to modify the surface since Au is well known for its ability to interact with range of ligands besides making structures bio-friendly. Ryan and co-workers have already reported such approach with semiconductor-gold hybrids where Cyt C proteins molecules were immobilized on Au via suitable ligands.[29] The Co and Co-core Au-shell nanomaterials are characterized by UV-visible spectroscopy,

Fluorescence spectroscopy, high resolution transmission electron microscopy (TEM), Fourier Transform Infrared (FTIR) spectroscopy and X-ray photoelectron spectroscopy (XPS). The magnetic property measurement using VSM reveals the retention of superparamagnetic character for the core-shell. Presented below are details of the investigation.

Experimental Section:

Materials: Cobalt chloride hexahydrate ($CoCl_2.6H2O$), sodium dodecyl sulfate (SDS) ($C12H_{25}NaO_4S$), oleic acid (9-octadecenoic acid), L-Tryptophan (Trp) ($C_{11}H_{12}N_2O_2$), sodium borohydride ($NaBH_4$) and Gold Chloride ($HAuCl_4$) were purchased from Sigma-Aldrich and SRL and as utilized as received.

Preparation of Co nanoparticles: In a typical experiment 10 mL of aqueous solution of $1x10^{-2}$ M cobalt chloride ($CoCl_2$) was taken with 10 mL aqueous solution of $1x10^{-1}$ M sodium dodecyl sulfate (SDS) and 1 mL methanolic solution of $1x10^{-2}$ M oleic acid. As the total volume of the aqueous solution had to be maintained at 100 mL so rest of the part was made up with double distilled water. Then 0.025 gm solid sodium borohydride ($NaBH_4$) was added to initialize the reduction of cobalt ions. After the addition of the reducing agent, as reduction was started so the solution turned into grayish black almost immediately. To assure the complete reduction, the solution was kept at ambient conditions for 2 hr. Then the blackish solution was allowed for repetitive centrifugation at 8000 rpm for 20 mins, followed by the separation of supernatant and pellet. Then the pellet obtained was washed with double distilled water and was re-centrifuged with the water under the above mentioned conditions. The pellet after second phase of centrifugation was processed suitably for the following characterizations such as UV-Vis spectroscopy, FTIR, TEM, ZETA potential measurement, XPS and VSM.

Preparation of Co-core Au-shell nanoparticles: After the formation of the Co nanoparticles, Trp was incorporated to modify the surface of the Co nanoparticles. For doing so, aqueous solution of L-Tryptophan was added to make the concentration of the overall solution $1x10^{-2}$ M. Various characterizations e.g. FTIR, UV-Vis spectroscopy, ZETA potential measurement, fluorescence spectroscopy were carried out at this stage of the process to ensure the incorporation of Trp. Then the Co nanoparticles were allowed to react with $1x10^{-3}$ M aqueous solution of $HAuCl_4$. Then the solution was stirred overnight and then centrifuged at 8000 rpm for 20 mins followed by the separation of supernatant and pellet, the pellet was collected and was separated for the various characterizations including magnetic measurements. The different steps of the reaction were presented in Scheme 1.

Scheme 1: Schematic representation of different steps involved in the synthesis of $Co_{core}Au_{shell}$ nanoparticle
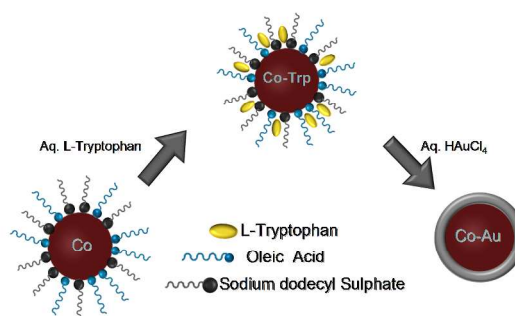
Characterization:

UV-Vis Spectroscopy: UV-Vis spectrum was recorded by Perkin-Elmer 25 Lambda UV-Vis Spectrometer to monitor the optical properties of Co-core and Co-core Au-shell nanoparticles solutions at a resolution of 1nm.

Fluorescence Spectroscopy: Fluorescence spectra was recorded by Perkin-Elmer LS55 fluorescence Spectrometer for Trp modified Co nanoparticles and thus for Co-core Au-shell nanoparticles.

Zeta Potential: Zeta potential was evaluated by Beckman COULTER DelsaTM NANO C particle analyzer to measure the zeta potential at surface of the three solutions at different steps.

Fourier Transform Infrared Spectroscopy: Fourier Transform Infrared (FTIR) spectroscopy was measured by Perkin-Elmer Spectrum 100 FT-IR Spectrometer at a resolution of 4 cm^{-1} to evaluate the bonding interaction at different steps after mixing the powder samples with potassium bromide. The FTIR spectrum of pure SDS, Oleic Acid and L-Tryptophan were recorded for comparison.

Transmission Electron Microscopy: Transmission electron microscopy (TEM) investigation was carried out by using FEI, Tecnai G2 F30, S-TWIN microscope operating at 300 kV. High-angle annular dark field scanning transmission electron microscopy (STEM-HAADF) employed here using the same microscope, which was equipped with a scanning unit and a HAADF detector from Fischione (model 3000). The compositional analysis was performed by energy dispersive X-ray spectroscopy (EDS, EDX Inc.) attachment on the Tecnai G2 F30. Energy-filtered TEM (EFTEM) measurements were carried out using GIF Quantum SE (model 963). Samples for these purposes were prepared by simple drop casting the solution on carbon coated copper grid and allowing the solutions to dry up.

X-ray Photoelectron Spectroscopy: X-ray photoelectron spectra (XPS) of the catalysts was recorded with custom built ambient pressure photoelectron spectrometer (APPES) (Prevac, Poland), equipped with VG Scienta's R3000HP analyzer and MX650 monochromator[30] Monochromatic Al Kα x-ray was generated at 450 W and used for measuring X-ray photoelectron spectrum

(XPS) of the above samples. Base pressure in the analysis chamber was maintained in the range of 2×10^{-10} Torr. The energy resolution of the spectrometer was set at 0.7 eV at a pass energy of 50 eV. Binding energy (BE) was calibrated with respect to Au $4f_{7/2}$ core level at 84.0 eV. The error in the reported BE values was within 0.1 eV. For peak synthesis, a mixed Gaussian-Lorenzian function with a Shirley type background subtraction was used. Samples were flooded with low energy electrons for efficient charge neutralisation.

Vibrating Sample Magnetometer: The magnetic measurements of the sample were performed by a superconducting quantum interference device vibrating sample magnetometer (SQUID-VSM, Quantum Design). The magnetization measurement dependent on both magnetic field and temperature had been performed. Field dependent magnetization (M-H) measurements of the sample had been made at 300K and 10K. Temperature dependent magnetization (M-T) measurements were performed at 150 Oe, 300 Oe and 600 Oe under zero field cool (ZFC) and field cool (FC) conditions.
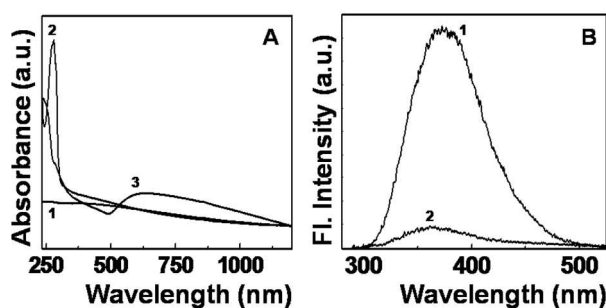
Results and discussion:

Fig. 1: (A) UV-Vis Spectra of Co (Curve 1), Trp modified Co (Curve 2) and $Co_{core}Au_{shell}$ nanoparticle (Curve 3) dispersed in aqueous medium. (B) Fluorescence Spectra of Trp modified Co (Curve 1) and $Co_{core}Au_{shell}$ nanoparticle (Curve 2) in aqueous medium.

It is interesting to mention here that cobalt nanoparticles prepared by the above mentioned technique, were stable against quick aerial oxidation probably due to the capping of surface ligands oleic acid and SDS. In this scenario transmetallation reaction could have been an effective method to generate core-shell structures.[31,32] This was a process where the shell materials could be deposited on the core by a galvanic exchange reaction between the two components. Definitely this method had several advantages. Oleic acid capped Co nanoparticles showed a negative value during the zeta potential measurement, Supporting Information SI-1. This hindered the approach of $AuCl_4^-$ to the cobalt surface when a transmetallation reaction was aimed. Due to adverse surface charge on the pristine cobalt nanoparticles, the surface was first modified with an amino acid L-Tryptophan (Trp) by stirring the Co nanoparticle solution with Trp overnight. The introduction of Trp changed the potential to positive, Supporting information SI-1. Trp had been already known not only for its ability to reduce $AuCl_4^-$ to Au^0 but also because of its capping efficiency for Au nanoparticles.[33] The modified Co nanoparticles were washed several times to avoid the presence of excess Trp in the medium which might act as nucleation points for discrete Au nanoparticles. The reduction of $AuCl_4^-$ to Au^0 was indicated by UV-Vis spectroscopy, Fig. 1A. The UV-Vis spectrum of the pristine oleic acid capped Co nanoparticles (Curve 1, Fig. 1A)

was almost featureless with a monotonic increase in the absorbance with decrease in wavelength and agreed well with those reported for Co nanoparticles.[34-37] Trp modified Co nanoparticles showed the characteristic absorption of Trp at 279 nm in the UV region (Curve 2, Fig. 1A).[38] This indicated the adsorption of the amino acid on Co surface. The development of a broad surface plasmon resonance peak centred around 606 nm (Curve 3, Fig. 1A) after the addition of aqueous $HAuCl_4$ to Trp modified Co nanoparticles was attributed to metallic gold in the nanoscale regime.[34] Moreover the photoluminescence (PL) spectra of Trp-Co nanoparticles showed appreciable intensity (Curve 1, Fig. 1B) at 374 nm when excited at 279 nm which was damped considerably (Curve 2, Fig. 1B) after the Au shell formation. The plausible cause could be efficient nonradiative decay after the formation of Au-shell and this observation was in good agreement with previous reports.[39-42] Apart from this, pristine cobalt nanoparticles did not have any signature of N (not shown in the paper), but for the core-shell structure showed N along with C, O, Co and Au in EDX analysis which clearly hinted towards the presence of Trp on surface of Co nanoparticles, Fig. 2A.
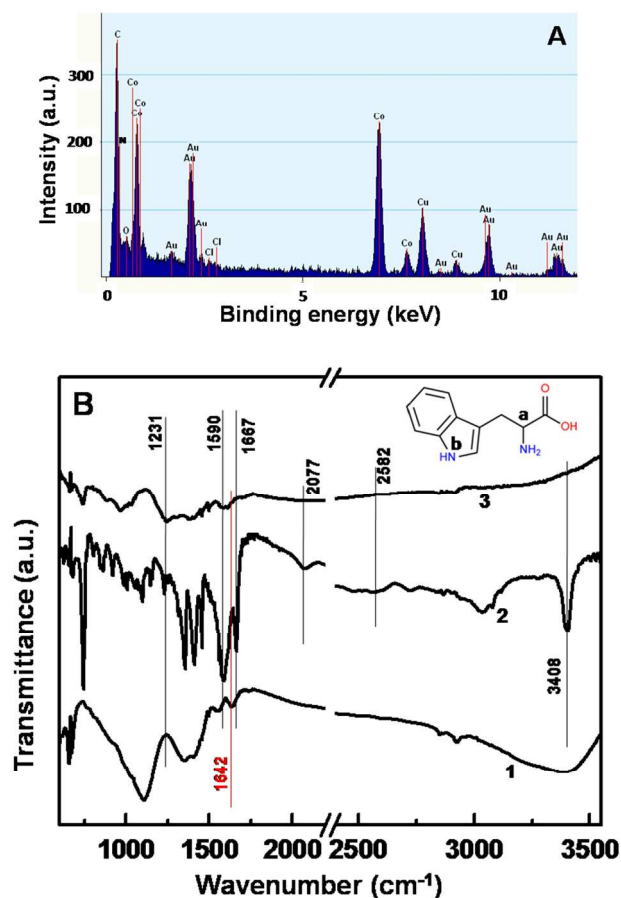

Fig. 2: (A) Spot EDX analysis of $Co_{core}Au_{shell}$ nanoparticles. (B) FTIR spectra of Co nanoparticle (Curve 1), Co after surface modification with Trp (Curve 2), and the same particle after formation of Au shell (Curve 3). (Inset B) Chemical Structure of L-Tryptophan.

The incorporation of amino acid Trp on the surface of Co nanoparticles was ensured from a detailed FTIR (Fig. 2B) and XPS (Fig. 3) results respectively. Thorough FTIR study revealed that carboxylic acid group of oleic acid had been shifted to 1642 cm^{-1}

compared to 1707 cm^{-1} for pure oleic acid due to interaction with cobalt nanoparticles, Curve 1, Fig. 2B.[43] The FTIR spectra changed drastically after the interaction with Trp, assured by the presence of bands characteristic of Trp at 1231, 1590, 1667, 2077, 2582 and 3408 cm^{-1} respectively, Curve 2, Fig. 2B. The terminal and indole amines groups of Trp were found to be relatively free along with a clear shift in asymmetric stretching of –COO- group from 1614 cm^{-1} (pure Trp)[44] to 1590 cm^{-1}. This indicated a direct interaction of carboxylic acid group of Trp to cobalt surface: the fact agreed well with the literature reporting a favorable interaction between cobalt/nickel nanoparticles and carboxylic acid group containing ligands.[45] The signatures of indole amine group at 2582 and 3408 cm^{-1} were damped considerably after the reduction of gold, this validated that reduction was initiated by amine group of the indole-ring, Curve 3, Fig. 2B.[33] The strong stretching frequency of amine group at 1667 cm^{-1} was also found to be transformed to a broad peak while –COO- stretching at 1590 cm-1 was found to be undisturbed.
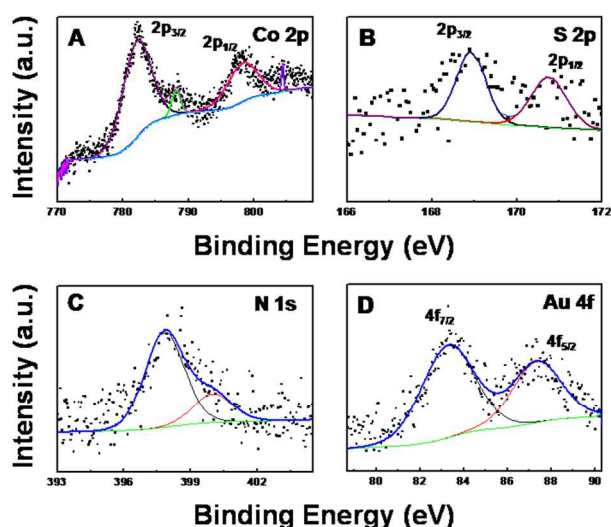

Fig. 3: XPS of (A) Co 2p (B) S 2p from Co nanoparticles and (C) N 1s, (D) Au 4f Co$_{core}$Au$_{shell}$ nanoparticles.

The proposition of incorporation of Trp and the formation of Au-shell was further validated by XPS analysis of the samples, Fig. 3. The core level binding energy (BE) of Co 2p$_{3/2}$ obtained from the pristine Co nanoparticles could be fitted to a single peak centered at 782.0 eV BE with a second component at 786.8 eV, Fig. 3A. The lower binding energy component (782.0 eV) was due to Co^0 states whereas the higher binding energy peaks might arise due to Co(OH)$_2$/CoO. The possibility of adsorbed Co^{2+}(oleate) complex on the surface of these nanoparticles could not be ignored which could also account for the shift to the higher BE. The similar results in XPS analysis were observed by Zanchet et al,[46] by Couto et al[47] for colloidal Ni synthesized via completely different routes but using oleic acid as capping agent and also by Gupta et al. for silver loaded by doxorubicin.[48] This agreed well with the FTIR observations. FTIR (Curve 1, Fig. 2B) indicated presence of –OH stretching frequency in the pristine cobalt along with the Co-oleic acid interaction. The feeble S 2p spectra was fitted into two spin orbit doublets at 168.8 and 170.7 eV BE, arising from S 2p$_{3/2}$ and S 2p$_{1/2}$ levels of −SO$_4$ group of SDS:[49] thus very minute amount of SDS was present on the surface, Fig. 3B. The

scenario changed considerably after the formation of Au-shell on Co nanoparticles. No signature of Co 2p was observed after core-shell formation. Basically, in XPS the electrons ejected from a point buried deeper from the surface experiences higher number of inelastic collisions than the surface electrons and thereby lost the energy to such an extent that they contribute exclusively to the low kinetic energy background. The results demanded metallic Co to be present away from the surface which had now been covered completely with metallic Au. On the other hand peaks of Au4f and N1s agreed well with the plausible mechanism of core-shell formation. The N1s spectrum was deconvoluted into two components at binding energy 397.8 and 399.9 eV, Fig. 3C. The lower binding energy peak corresponded to first amine group (inset, Fig. 2B) and the higher one to the 2nd amine group which was attached to the indole ring of Trp, adsorbed on the surface of Co-Au hybrid nanoparticles.[50] The XPS of Au 4f$_{7/2}$ and 4f$_{5/2}$ spin orbit core levels (Fig. 3D) of Co-core Au-shell nanoparticles were observed at centered at 84.0 eV and 87.7 eV BE with a energy gap of 3.7 eV between them. This undoubtedly corresponded to Au^0 state.[51] This authenticated our proposition of complete reduction of chloroaurate ions in presence of Trp.
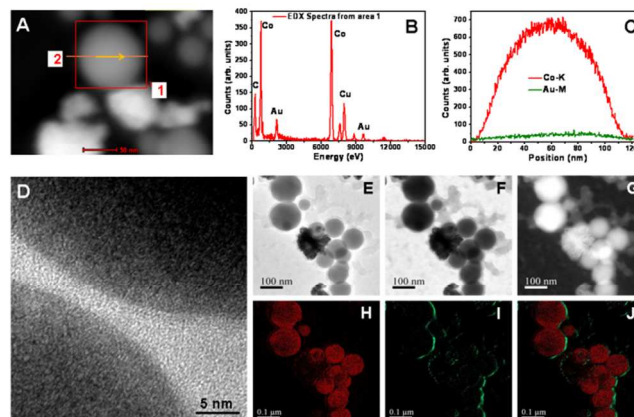

Fig. 4: TEM images of Co$_{core}$Au$_{shell}$ nanoparticle (A,D-J), (B) Spot EDX analysis of the same core and shell regions obtained from the area which are shown in the above figures, showing the core-shell morphology, (C) Chemical mapping of a single nanoparticle highlighted in image (A).

Structural information was obtained using TEM. The pristine Co nanoparticles were shown in Supporting Information SI-2. The size distribution of the same was presented in Supporting Information SI-3 as obtained from both TEM and DLS data. To investigate the chemical composition of the core-shell structure, we performed STEM-HAADF analysis. It provided the Z-contrast image, where the intensity of scattered electrons is proportional to the square of the atomic number Z. Fig. 4A depicted the HAADF-STEM image of a Co/Au core-shell nanoparticle. EDX spectra from area 1 in Fig. 4A was plotted in 4B. The spatial distributions of the atomic contents across the Co/Au core-shell nanoparticle were obtained using energy dispersive X-ray spectroscopy (EDX) line profile. Fig. 4C showed the EDX profiles for Co, and Au across the line 2 as shown in Fig. 4A. The high concentration of Co in the cores and the tendency for Au accretion to form a shell was clearly visible by a highly magnified bright field TEM image, (Fig. 4D). For a detailed distribution of Co, and Au in core-shell

nanoparticle, we had performed the elemental mapping using EFTEM as illustrated in Fig. 4E-J. Energy filtered images were acquired using a contrast aperture of about 10 mrad to reduce aberrations (mostly chromatic). Chemical maps from Co M (60 eV), and Au O (54 eV) edges were obtained using jump-ratio method by acquiring two images (one post-edge and one pre-edge), respectively, to extract the background, with an energy slit of 4 eV for Co and Au. The composite image in Fig. 4J gave a clear confirmation of the core-shell structure and elemental composition spatially separated. EDX data (Fig. 4C) obtained for these hybrid particles suggested the presence of thin Au-shell on Co-core. All these images provided strong concurrent evidence for the core-shell structure.
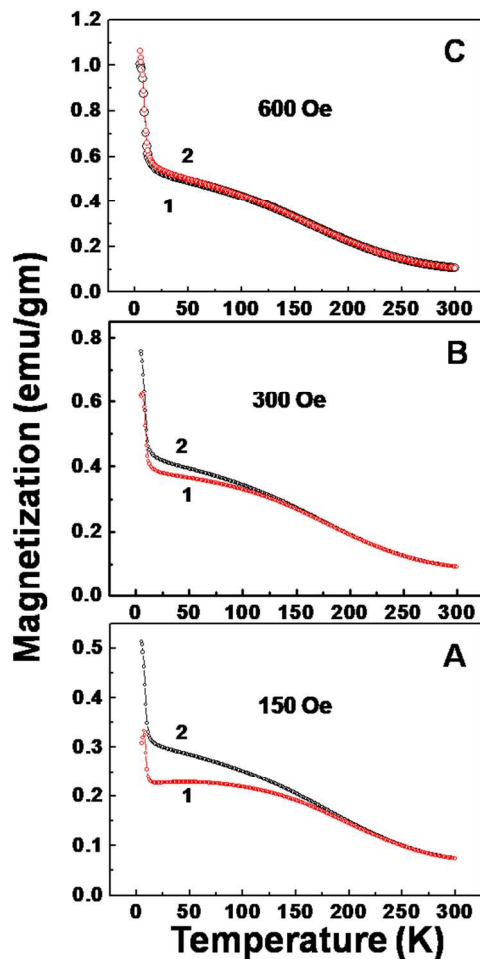

Fig. 5: Temperature dependent magnetization of $Co_{core}Au_{shell}$ nanoparticle. The applied magnetic field was (A) 150 Oe. (B) 300 Oe. (C) 600 Oe.

The temperature dependence of the magnetization for the $Co_{core}Au_{shell}$ nanoparticles was shown in Fig. 5 where the applied magnetic field was kept at three different values of 150 Oe, 300 Oe and 600 Oe respectively. The temperature was varied between room temperature 300 K and 5 K. Curve 1 in Fig. 5A, 5B and 5C corresponded to the magnetization against temperature (M-T) plot under ZFC condition while Curve 2 was the measurement carried out under FC condition. As could be clearly seen, the curves of temperature dependent ZFC and FC magnetizations were typical of

magnetic nanoparticles. Magnetic particles below a certain size regime behaved as superparamagnetic with characteristic features: i) magnetization under ZFC condition measured using low magnetic fields, displayed a maximum at a certain temperature, called the blocking temperature, T_B ii) a divergence in the magnetization curves measured under ZFC and FC conditions below the blocking temperature and iii) magnetic hysteresis loop and remnant magnetization below T_B whereas hysteresis behaviour disappeared above T_B.

The core-shell particles showed a divergence between the magnetization curves measured under ZFC and FC conditions up to 187K when the applied field is 150 Oe. The magnetization curves with increasing field of 300 Oe diverged at relatively lower temperature of 132K, in Fig. 5B whereas these two curves remained superimposed within the range of experimental temperature when the applied field was kept at 600 Oe, (Fig. 5C). Actually bifurcation of magnetization curves measured under ZFC and FC conditions should occur at relatively lower temperature with increasing magnetic field i.e. there would be a clear gradual lower temperature shift in T_B on increasing the applied field. This too was consistent with signature of superparamagnetic nature of the sample. Generally for superparamagnetic system at very low temperature spins were aligned and hence represented a frozen condition. Gradual increase in thermal excitation in presence of mild applied magnetic field, parallel spin orientation build up in the system resulting in an augmentation in magnetization value. Then the system attained a highest magnetization at a particular temperature (blocking temperature, T_B). Thermal excitation and low applied magnetic field both played significant role in orienting the spins or rather reaching the maximum magnetization. Further on increasing the applied magnetic field (from 150 Oe to 300 Oe to 600 Oe) it became easier to achieve the maximum parallel spin orientation (maximum of magnetization) and hence observed a shift in T_B at lower temperature. This nature was pretty clearly demonstrated in Fig. 5. But at low temperature (below 25 K) there was a sudden increase in magnetic moment. It might indicate the presence of free paramagnetic spins in the system. The blocking temperature was actually related to the size of the magnetic particles and the magnetocrystalline anisotropy constant (K) by the equation $K = 25k_BT_B/V$ where the k_B and V were the Boltzmann constant and the volume of single particle, respectively and T_B was the blocking temperature. By substituting the values for a ~77.3 nm (average particle size obtained from particles size distribution calculation from TEM images, Supporting Information SI-4) particle we deduced K to be 26.7×10^2 erg cm^{-3}, which was found to be much lower than bulk cobalt (45×10^5 erg cm^{-3}).[52] The difference between the values was expected as we calculated K using the average particle size and not the individual crystallite size which actually controlled the individual magnetic directions of the grains and hence the blocking temperature. It was noteworthy that magnetic core was isolated in the diamagnetic gold shell, but the magnetization curves under ZFC and FC conditions were devoid of a clear blocking temperature at very low applied magnetic field, due to slight polydispersity in particle size. Apart from this, several other phenomenon related to the nanoscale regime such as the structural disorder, surface anisotropy, non-magnetic or weak magnetic interfaces, the lack of surface coordination for the surface magnetic atoms and the electron exchange between the capping agent and surface atoms were also known to influence the magnetic properties.[53] One or several of these phenomena in tandem could also had led to the smaller values of the magnetic parameters in our systems.

The field dependent magnetic behaviour data, measured at 10 K (below the blocking temperature, Fig. 6a) and at 300 K (well

above the blocking temperature, Fig. 6b) were displayed in Fig. 6. It clearly indicated strong hysteresis nature at low temperature (10K) and weak hysteresis nature at room temperature (300K), which indicated that the system possesses ferromagnetic (FM) ordering. In the high field region M-H curves indicated that the magnetic moments were unsaturated. It might be due to coexistence of paramagnetic (PM) phase along with the ferromagnetic (FM) phase.[54] Typically the feature observed in the M-H curves was in accordance with those expected for superparamagnetic nano particles. The M-H curves of the sample at both 10K and 300K did not fit well with the Brillouin-function as should be the case of purely PM or FM system. But it fits quiet well with equation (1) given below[55]

$$M(H) = (2M_{FM}^{S}/\text{л})\tan^{-1}[(H\pm H_{ci})/H_{ci}\tan\{(\text{л }M_{FM}^{R})/2\ M_{FM}^{S}\}] + \chi H \qquad(1)$$

Respaud *et al*[52] described equation (1) consisted of FM as well as PM components where M_{FM}^{S}, M_{FM}^{R}, H_{ci} and χ were saturation magnetization, remanent magnetization the intrinsic coercivity, and PM susceptibility. Subtracting the PM parts from the experimental data, saturation of magnetization in the high field region could be observed (as indicated by the red lines in Fig. 6). The saturation magnetic moment below blocking temperature (10K) was significantly high (nearly 10 ten times or I order of magnitude) in comparison to saturation magnetic moment above blocking temperature (300K). This type of significant or complete depletion of ferromagnetism above blocking temperature was quite familiar feature for superparamagnetic nanoparticles.[56] The estimated ratio of FM to PM contributions at 10K was calculated to be 0.661 and the ratio remained same (within the experimental and calculation error) at 300K, the exact calculated value was found to be 0.667. Both calculation was performed at H=4000 Oe. It was indicative of regular tendency of magnetization and confirmed the absence of carrier or rather defect mediated FM nature of the sample.[57] The constancy of the ratio of FM to PM moments at 10K and 300K suggested that FM ordering originated from Co-Au core shell structure and indeed reflected superparamagnetic nature of Co nanoparticles.
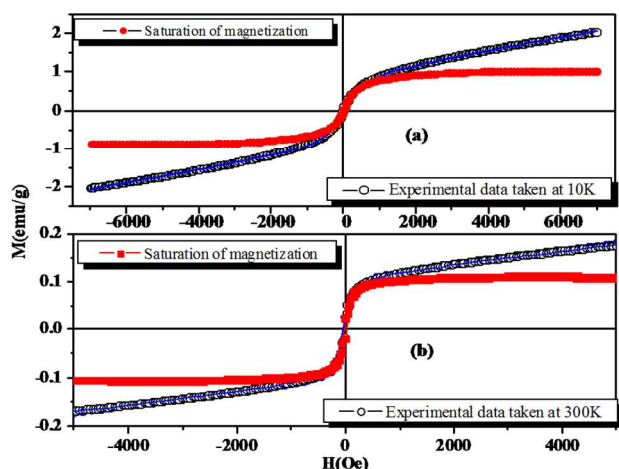

Fig. 6: Magnetization against magnetic field (M-H) variation at (a) 10K and (b) 300 K. The solid blue line represents the theoretical fit of the experimental MH curves. The red data points represent saturation magnetization after subtraction of paramagnetic contributions from the experimental data points.

Conclusion:

An easy and effective method for the synthesis of cobalt-core gold-shell nanoparticles had been reported at an ambient temperature. Cobalt nanoparticles prepared were initially capped with surfactants and hindered the approach of $AuCl_4^-$ for transmetallation. Thus the system behaved differently from its analogous Co-core Ag-shell hybrids where surfactants capped Co nanoparticles could be used directly for transmetallation with Ag^+. A minor but extremely effective surface modification of cobalt nanoparticles was successfully achieved to facilitate Au-shell formation : a comparative investigation is in progress. More importantly the synthetic strategy mentioned here, was purely water based and did not involve costly and/or toxic chemicals at any stage of the process. This definitely evoked potential applications including biological systems. The magnetic characteristics of the hybrid nanoparticles were studied in great details and were found to be in accordance with those expected for nanoscale superparamagnetic particles. The blocking temperature where the magnetic directions of individual grains essentially remain invariant was determined to be ~187K for these particles at an applied field of 150 Oe which shifted to relatively lower temperature with the increase in the applied external field.

Notes and references

[a]Department of Chemistry, University of Calcutta, 92 A.P.C. Road, Kolkata: 700009, India
[b]CRNN, University of Calcutta, JD 2, Sector III, Salt Lake, Kolkata: 700098, India
[c]Department of Physics, University of Calcutta, 92 A.P.C. Road, Kolkata: 700009, India
[d]Surface Physics Division, Saha Institute of Nuclear Physics, 1/AF Bidhannagar, Kolkata-64, India
[e]Catalysis Division and Center of Excellence on Surface Science, CSIR – National Chemical Laboratory, Dr. Homi Bhabha Road, Pune -411 008, India

*To whom correspondence should be addressed: E-mail: tanushreebala@gmail.com

References:

1 F. Mafuné, Jun-Ya Kohno, Y. Takeda and T. Kondow, *J. Phys. Chem. B.*, 2002, **106**, 7575.
2 S. L. Westcott, S. J. Oldenburg, T. R. Lee and N. J. Halas, *Langmuir,* 1998, **14**, 5396.
3 H. Z. Zhang, Y. C. Kong, Y. Z. Wang, X. Du, Z. G. Bai, J. J. Wang, D. P. Yu, Y. Ding, Q. L. Hang and S. Q. Feng, *Solid State Communications,* 1999, **109**, 677.
4 K. K. Caswell, C. M. Bender and C. J. Murphy, *Nano Lett.,* 2003, **3**, 667.
5 A. Ghezelbash, M. B. Sigman, Jr. and B. A. Korgel, *Nano Lett.,* 2004, **4**, 537.
6 X. Guo, Q. Zhang, Y. Sun, Q. Zhao, J. Yang, *ACS Nano,* 2012, **6**, 1165.

7 G. K. Joshi, K. A. Smith, M. A. Johnson and R. Sardar, *J. Phys. Chem. C. ,* 2013, **117**, 26228.

8 J. H. Jung, G. B. Hwang, J. E. Lee and G. N. Bae, *Langmuir,* 2011, **27**, 10256.

9 Y. Song, J. Ding and Y. Wang, *J. Phys. Chem. C.,* 2012, **116**, 11343

10 M. Rubio-Roy, O. Vlasin, O. Pascu, J. M. Caicedo, M. Schimdt, A. R. Goñi, N. G. Tognalli, A. Fainstein, A. Roig and G. Herranz, *Langmuir,* 2012, **28**, 9010.

11 E. Petryayeva and U. J. Krull, *Analytica Chimica Acta,* 2011, **706**, 8.

12 M. B. Cortie and A. M. McDonagh, *Chem. Rev.,* 2011, **111**, 3713.

13 Myung-Gil Kim, J. W. Hennek, H. S. Kim M G. Kanatzidis, A. Facchetti and T. J. Marks, *J. Am. Chem. Soc.,* 2012, **134**, 11583.

14 M. Zahmakiran and S. Özkar, *Nanoscale,* 2011, **3**, 3462.

15 J. Liu, S. Z. Qiao, J. S. Chen, X. W. Lou, X. Xing and G. Q. Lu, *Chem. Commun.,* 2011, **47**, 12578.

16 Y. Bao, H. Calderon and K. M. Krishnan, *J. Phys.Chem. C.,* 2007, **111**, 1941.

17 M. Radisic, R. K. Layer and S. K. Murthy, *Int J Nanomedicine,* 2006, **1(1)**, 3.

18 T. D. Schladt, K. Schneider, H. Schild and W. Tremel , *Dalton Trans.,* 2011, **40**, 6315.

19 T. Hyeon, *Chem. Commun.,* 2003, 927.

20 H. She, Y. Chen, X. Chen, K. Zhang, Z. Wang, Dong-Liang Peng, *J. Mater. Chem.,* 2012, **22**, 2757.

21 OV Salata, *Journal of Nanobiotechnology,* 2004, **2**.

22 S. V. Kershaw, A. S. Susha and A. L. Rogach, *Chem. Soc. Rev.,* 2013, **42**, 3033.

23 D. L. Pérez, A. Espinosa, L. Martínez, E. Román, C. Ballesteros, A. Mayoral, M. García-Hernández and Y. Huttel,*. J. Phys. Chem. C.,* 2013, **117**, 3101.

24 D. S. Sidhaye, T. Bala, S. Srinath, H. Srikanth, P. Poddar, M. Sastry and B. L. V Prasad, *J. Phys. Chem. C.,* 2009, **113**, 3426.

25 J. F Godsell, T. Bala, K. M. Ryan and S. Roy, *J. Phys. D: Appl. Phys.,* 2011, **44**, 325004.

26 E. Girgis, W. K. B. Khalil, A. N. Emam, M. B. Mohamed and K. V. Rao, *Chem. Res. Toxicol,* 2012, **25**, 1086.

27 N. Dahal and V. Chikan, *Inorg. Chem..,* 2012, **51**, 518.

28 Z. Lu, M. D. Prouty, Z. Guo, V. O. Golub, C. S. S. R. Kumar and Y. M. Lvov, *Langmuir,* 2005, **21**, 2042.

29 C. O'Sullivan, S. Crilly, F. R. Laffir, A. Sing, E. Magner and K. M. Ryan, *Chem. Commun.,* 2011, **47**, 2655.

30 K. Roy, C. P. Vinod and C. S. Gopinath, *J. Phys. Chem. C.,* 2013, **117**, 4717.

31 PR. Selvakannan and M. Sastry, *Chem. Commun.,* 2005, 1684.

32 Woo-ram Lee, M. G. Kim, Joon-rak Choi, Jong-II park, S. J. Ko, S. J. Oh and J. Cheon, *J. AM. CHEM. SOC.,* 2005, **127**, 16090.

33 PR. Selvakannan, S. Mondal, S. Phadtare, A. Gole, R. Pasricha, S. D. Adyanthaya and M. Sastry. *Journal of Colloid and Interface Science,* 2004, **269**, 97.

34 J. A. Creighton and D. G. Eadon, *J. Chem. Soc., Faraday Trans*., 1991, **87**, 3881.

35 C.F. Bohren and D.R. Huffman, Wiley Vch, ISBN 978-0-471-29340-8, 1998, pp 130-154

36 Challa S.S.R. Kumar, Springer, ISBN 978-3-642-27593-7, 2013, pp 231-285

37 Z. Kaminskiene, I. Prosycevas, J. Stonkute and A. Guobiene, Acta Physica Polonica A, 2013, **123**, 111.

38 S. W. Lin, T. P. Sakmar, *Biochemistry,* 1996, **35**, 11149.

39 P. Joshi, V. Shewale, R. Pandey, V. Shanker, S. Hussain, S. P. Karna, *J. Phys. Chem. C*., 2011, **115**, 22818.

40 S. H. D. P. Lacerda, J. J. Park, C. Meuse, D. Pristinski, M. L. Becker, A. Karim and J. F. Douglas, *ACS Nano,* 2010, **4**, 365.

41 P. Joshi, S. Chakraborty, S. Dey, V. Shanker, Z. A. Ansari, S. P. Sing and P. Chakrabarti, , *Journal of Colloid and Interface Science*, 2011, **355**, 402.

42   S. Chakraborty, P. Joshi, V. Shanker, Z. A. Ansari, S. P. Sing and P. Chakrabarti, *Langmuir,* 2011, **27**, 7722.

43 T. Bala, S. K. Arumugam, R. Pasricha, B. L. V. Prasad and M. Sastry, *J. Mater. Chem..,* 2004, **14**, 1057.

44 Z. Zhengbin, W. Wei, L. Liansheng, F. Youjun and W. Zhijian, *Journal of Colloid and Interface Science,* 1997, **190**, 1.

45 N. Wu, L. Fu, M. Su, M. Aslam, K. C. Wong and V. P. Dravid, , *Nano Lett.,* 2004, **4**, 383.

46 H. Winnischofer, T. C. R. Rocha, W. C. Nunes, L. M. Socolovsky, M. Knobel and D. Zanchet, *ACS Nano,* 2008, **2**, 1313.

47 G. G. Couto, J. J. Klein, W. H. Schreiner, D. H. Mosca, A. J. A. de Oliveira and A. J. G. Zarbin, *Colloid Interface Sci.,* 2007, **311**, 461.

48 N. R. Gupta, B.L.V. Prasad, C. S. Gopinath and M.V. Badiger, *RSC Adv.,* 2014, **4**, 10261

49 M. Sathish, R.P. Viswanath and C.S. Gopinath, *J. Nanosci. Nanotech*., 2009, **9,** 423.

50 C. S. Gopinath, *J. Phys. Chem. B.,* 2006, **110**, 7079.

51 A. C. Sunilsekhar, K. Sivaranjani, C. S. Gopinath, and C.P. Vinod, *Catal. Today,* 2012, **198,** 92.

52 B. D. Cullity, Introduction toMagnetic Materials, Addison-Wesley Publishing, Reading, MA, 1972.

53 S. Singamaneni, V. N. Bliznyuk, C. Binek and Y. Tsymbal, *J. Mater. Chem..,* 2011, **21**, 16819.

54 T. Meron and G. Markovich, *J. Phys. Chem. B*., 2005, **109**, 20232.

55 M. Respaud, J. M. Broto, H. Rakoto, A. R. Fert, L. Thomas, B. Barbara, M. Verelst, E. Snoeck, P. Lecante, A. Mosset, J. Osuna, T. C. Ould, C. Amiens and B. Chaudret, *Phys. Rev. B.,* 1998, **57,** 2925.

56 C. Pereira, A. M. Pereira, P. Quaresma, P. B. Tavares, E. Pereira, J. P. Araújo and C. Freire, *Dalton Trans.,* 2010, **39**, 2842.

57 S. K. Neogi, S. Chattopadhyay, R. Karmakar, A Banerjee, S. Bandyopadhyay and A Banerjee, *Journal of Alloys Compounds*, 2013, **573**, 76.

A facile method for synthesis of Co-core Au-shell nanohybrid

Debasmita Sardar, S. K. Neogi, S. Bandyopadhyay, Biswarup Satpati, Tanushree Bala

$Co_{core}Au_{shell}$ nanoparticles